Research Article | Vol. 26, No. 21 | 15 Oct 2018 | OPTICS EXPRESS 27127
Optics EXPRESS

Enhanced fault characterization by using a conventional OTDR and DSP techniques

MANUEL P. FERNÁNDEZ,[1,2,3,*] LAUREANO A. BULUS ROSSINI,[1,2,3] JUAN PABLO PASCUAL,[1,2,3] AND PABLO A. COSTANZO CASO[1,2,3]

[1]*LIAT - Laboratorio de Investigación Aplicada en Telecomunicaciones (CNEA, Comisión Nacional de Energía Atómica), Av. Bustillo 9500, Bariloche 8400 (RN), Argentina*
[2]*CONICET, CCT Patagonia Norte, Bariloche 8400 (RN), Argentina*
[3]*Instituto Balseiro (UNCuyo-CNEA), Bariloche 8400 (RN), Argentina*
**manuel.fernandez@ib.edu.ar*

Abstract: To plan a rapid response and minimize operational costs, passive optical network operators require to automatically detect and identify faults that may occur in the optical distribution network. In this work, we present DSP-Enhanced OTDR, a novel methodology for remote fault analysis based on conventional optical time-domain reflectometry complemented with reference traces and DSP-based techniques. We first obtain the optimal decision thresholds to detect deviations in the noisy OTDR measurement. In order to quantify and characterize the fault, the detection stage is followed by one of estimation where its return loss and insertion loss are determined. We experimentally demonstrate that this approach allows to detect and characterize faults with an accuracy higher than that found in conventional OTDR trace analysis. In our experiments, we achieved detection sensitivities higher than 0.2 dB in a 1:16 split-ratio PON, and higher than 1 dB in a 1:64 split-ratio PON, achieving estimation errors that can be as low as 0.01 dB. We also verified how the optical network terminal's reflectivity can improve the detection capabilities.

1. Introduction

Passive optical networks (PON) are cost-efficient solutions to deliver a fiber connection to the users and they have been massively deployed in recent years [1]. Consequently, to maintain service reliability, physical layer monitoring of these networks is extremely important. Firstly, a complete monitoring system must allow the automatic detection and localization of events that may occur in the optical distribution network (ODN) in favor of operational expenditures (OPEX) savings by avoiding the need for in-field testing [2]. Moreover, it must timely detect and characterize different faults to plan a quick response, minimizing the mean down time, which affects the customers' satisfaction. In addition, the monitoring solution should involve low capital expenses (CAPEX) and it must be easily installed in already deployed PONs [3].

The use of an optical time-domain reflectometer (OTDR) is the most efficient technique to characterize an optical link [4,5]. However, the direct application of OTDR in PONs presents severe limitations: the OTDR waveform is composed by the addition of backscattering from several distribution drop fibers (DDF) and hence the real magnitude and localization of the fault is missed. Since reflections arising from several branches are expected, the event dead zone becomes critical. In addition, power splitters reduce the backscattered power and hence the accuracy of the fault characterization is limited.

Several OTDR-based techniques have been proposed to overcome the aforementioned limitations. Some of them rely on the use of reflective filters [6,7] and optical encoders [8–12] as demarcation devices. Others use a tunable OTDR together with multiplexers as a passive bypass in the remote node in order to assign a monitoring wavelength to each branch [13,14] or group of branches [15]. To achieve higher dynamic range, more complex OTDR structures have been studied, such as Coherent-OTDR [16], Correlation [17] and Chaos-based OTDR [18], and Photon-counting OTDR [19,20].

#331793 https://doi.org/10.1364/OE.26.027127
Journal © 2018 Received 18 May 2018; revised 27 Jul 2018; accepted 29 Jul 2018; published 3 Oct 2018

Optics EXPRESS

Although the mentioned proposals can have an improved performance over a commercial OTDR device, it is extremely important and desirable from an operators' point of view to exploit the advantages of the remote monitoring with conventional OTDR and digital signal processing (DSP) techniques: i.e., simplicity, low-cost, scalability and ease of implementation in already operative PONs. Hence, in this work we present a novel methodology for fault analysis in OTDR profiles, which we called DSP-Enhanced OTDR (DSPE-OTDR). In this approach, we employ a conventional OTDR, which yields a typical measurement trace, followed by a novel and specific algorithm that characterizes the fault and identifies the branch to which it belongs. The event detection algorithm based on the Neyman-Pearson criterion is applied to the comparison of the acquired measurement with a reference one, obtained during the normal operation of the network. We derive explicit equations for the optimal thresholds and the detection and false alarm probabilities, and we carry out a comprehensive performance evaluation as a function of the OTDR characteristic parameters. The detection stage is followed by a maximum-likelihood estimation process to obtain the event parameters, which allows to remotely characterize and identify the type of fault with an accuracy higher than that achieved by simply comparing the two measurements as is the case of conventional OTDRs.

The present work is organized as follows. In Section 2 the fundamentals of the DSPE-OTDR and the mathematical formalism for the acquired signals are introduced. From these models, Sections 3 and 4 describe the detection and estimation algorithms, respectively. The experiments that demonstrate the algorithm's effectiveness are carried out in Section 5. Finally, Section 6 covers the considerations that have to be taken in a multiple-fault scenario.

2. Fundamentals of DSPE-OTDR for PON monitoring

2.1 Description

We assume a star topology for the PON, such as that illustrated in Fig. 1(a). The ODN is composed by a feeder fiber, a 1:*N* power splitter and *N* drop fibers connected to it, which derive the data signals to *N* optical terminals. The OTDR is connected to the PON through a wavelength multiplexer to be completely transparent to the data signals.

The operation of the remote monitoring scheme based on the DSPE-OTDR is depicted in Fig. 1(b). After the current measurement is obtained, a detection and coarse identification stage compares the acquired signal $y(z)$ with a reference measurement $y_{REF}(z)$, obtained during normal operation. From this, the new events are identified at a given distance from the input terminal. The detection stage compares the acquired noisy measurement to a couple of predefined thresholds. Then, two binary decisions are made for each sample:

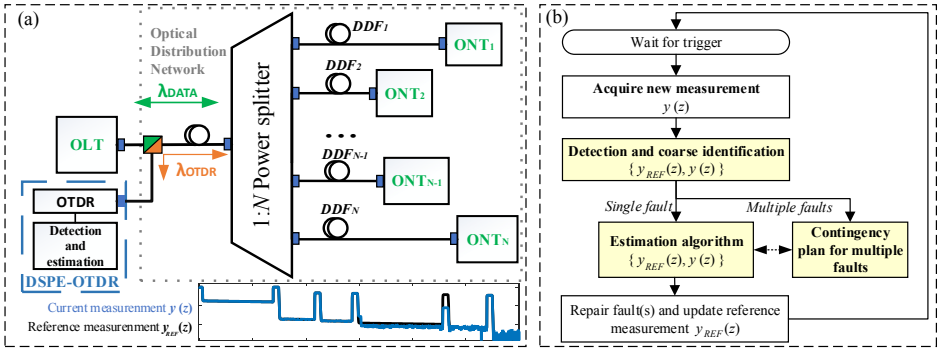

Fig. 1. (a) Scheme of OTDR-based monitoring system and (b) operation of the DSPE-OTDR.

(a) *there is* / *there is not* a reflection.

(b) *there is* / *there is not* a loss.

Optics EXPRESS

The next step involves the fault characterization. When a single fault is identified, which is the scenario with the highest probability of occurrence, its characteristic parameters, such as return loss and insertion loss, are estimated from the samples where reflections and losses were detected, respectively. The detection and estimation will be addressed in Sections 3 and 4.

On the other hand, when multiple simultaneous faults are identified, an alternative contingency plan for multiple events is initiated. In this case, the estimation algorithm must take into account different scenarios, which will be discussed in Section 6, in order to apply the estimation criteria in an adequately sequenced fashion.

2.2 Mathematical model for the OTDR signal

Before describing the detection and estimation procedure in detail, it is necessary to briefly introduce well-known concepts of OTDR, in order to better understand the proposed method and its fundamentals.

To obtain an algebraic expression for the acquired OTDR measurement at a given sample $z = z_i$ we firstly define the following variables and parameters:

- K is the fiber backscattering factor and α is the fiber attenuation constant.
- The reference measurement at z_i is $y_{REF}(z_i)$, which has contributions from several DDFs.
- The probe pulse has a peak power P_0 and temporal width T, i.e. spatial width $W \equiv Tv_g / 2$.
- The e-th drop fiber, DDF$_e$, has its branch termination at a distance $z = z_{\mathrm{ONT}e}$ from the OTDR input terminal.
- The total round-trip insertion loss and power penalties at a distance z_i in the DDF$_e$ under normal operation is f_e.

We next describe the mathematical model for the acquired signal after a fault has occurred in the DDF$_e$. Let us consider the event is localized at a distance z_e and it is characterized by a return loss RL_e and an insertion loss IL_e (both expressed in dB). The acquired signal after the fault occurrence $y(z)$ will show deviations with respect to the reference signal, where two classes of deviations are considered, namely reflections and losses.

Assuming that the Fresnel-reflected power is much larger than the backscattering power, when a reflective event with return loss RL_e occurs at a distance z_e, the detected signal at the sample $z_i \in (z_e - W/2, z_e + W/2)$ can be expressed in terms of the reference signal as

$$y_R(z_i) = y_{REF}(z_i) + f_e \frac{1}{N^2} 10^{-\frac{2\alpha z_e}{10}} P_0 10^{-\frac{RL_e}{10}}. \tag{1}$$

In the case of the loss, the backscattering from the DDF$_e$ drops proportionally to twice IL_e, and the detected signal evaluated at a z_i behind the loss-inducing event, can be expressed as

$$y_L(z_i) = y_{REF}(z_i) + f_e \frac{1}{N^2} 10^{-\frac{2\alpha z_i}{10}} P_0 W K \left(10^{-\frac{2IL_e}{10}} - 1 \right), \tag{2}$$

Optics EXPRESS

where the term $10^{-\frac{2IL_e}{10}}-1<0$. When the observation sample corresponds to the ONT reflective termination of the DDF$_e$, localized at $z_i \in (z_{\mathrm{ONT}e}-W/2, z_{\mathrm{ONT}e}+W/2)$ and assuming that the reflected power is much larger than the backscattered power, the detected signal can be written in terms of the reference signal as

$$y_L(z_i) = y_{REF}(z_i) + f_e \frac{1}{N^2} 10^{-\frac{2\alpha z_{\mathrm{ONT}e}}{10}} P_0 10^{-\frac{RL_{\mathrm{ONT}e}}{10}} \left(10^{-\frac{2IL_e}{10}}-1\right). \quad (3)$$

The latter expression is highly relevant since its consideration greatly enhances the detection algorithm performance, as it will be shown in Section 3.2.

2.3 Noise considerations

Each sample in the acquired signal contains a random noise term $y_N(z_i)$ added to the signal whose statistics define the detection approach. On one hand, commercial OTDRs use laser diodes that have linewidths of several nanometers, which lead to low coherence lengths compared to the pulse width, and hence, coherent Rayleigh noise is negligible. On the other hand, since several hundreds of averages are performed it is reasonable to assume that the noise follows a Gaussian distribution. Therefore, the resulting noise term can be accurately modeled as an additive Gaussian random variable with zero-mean and variance σ_N^2 [5,21].

It should be remarked that the detection algorithm described here is aimed to be used with conventional OTDR devices. For other OTDR configurations, their intrinsic noise statistics should be taken into account (e.g. the Poisson noise in photon-counting OTDR and the coherent Rayleigh noise in Coherent-OTDR [20]). In addition, this presented detection approach can be extended to other configuration such as φ-OTDR for sensing applications [22].

3. DSPE-OTDR: event detection

In this section, we introduce how the DSPE-OTDR identifies the faults by providing a summarized but comprehensive mathematical formalism. Firstly, we derive the event detection algorithm from which we obtain the required decision thresholds. The acquired OTDR noisy measurement is then compared to the thresholds in order to identify reflections and losses. After that, we evaluate the performance of the detection algorithm, which allows to define the OTDR acquisition parameters needed to achieve a given sensitivity.

3.1 Detection algorithm

Each sample of the OTDR acquired signal $y(z_i)$ is a random variable with normal distribution (since the noise is Gaussian with zero-mean and variance σ_N^2). The detection procedure is then divided into two hypothesis tests:

(a) *Decide between* H_R *and* H_0.

(b) *Decide between* H_L *and* H_0.

Under the null hypothesis, H_0, neither reflection nor loss are present with respect to the reference measurement. Under the hypotheses H_R and H_L, the measurement presents a reflection or a loss, respectively. Therefore, the hypotheses can be summarized as

$$\boldsymbol{H_0} \rightarrow y(z_i) \sim \mathcal{N}\left(y_{REF}(z_i), \sigma_N^2\right) \qquad \boldsymbol{H_k} \rightarrow y(z_i) \sim \mathcal{N}\left(y_k(z_i), \sigma_N^2\right) \quad (4)$$

Optics EXPRESS

where $k = R, L$ and $\mathcal{N}\left(\mu, \sigma^2\right)$ indicates the normal distribution with mean μ and variance σ^2.

To design the detection tests we follow the Neyman–Pearson criterion [23], where the decision rules are designed to maximize the probability of detection, P_D^k, under the constraint that the probability of false alarm, P_{FA}^k, does not exceed a given value. The derivation of the detection tests lead to the following decision rules

$$y(z_i) \underset{H_0}{\overset{H_R}{\gtrless}} \eta_R(z_i) \qquad y(z_i) \underset{H_L}{\overset{H_0}{\gtrless}} \eta_L(z_i), \tag{5}$$

where η_R and η_L are the threshold for the reflection and the loss tests, respectively. Figure 2 depicts the decision regions and the detection and false alarm probabilities for both tests. The probabilities of false alarm can be written as

$$P_{FA}^R = Q\left(\frac{\eta_R - y_{REF}}{\sigma_N}\right) \qquad P_{FA}^L = 1 - Q\left(\frac{\eta_L - y_{REF}}{\sigma_N}\right), \tag{6}$$

where $Q(x)$ is the Q-function. Thus, we propose to obtain the decision thresholds in Eq. (5) from Eq. (6) by fixing a P_{FA}. Once the thresholds are defined, the probability of detection is

$$P_D^R = Q\left(\frac{\eta_R - y_R}{\sigma_N}\right) \qquad P_D^L = 1 - Q\left(\frac{\eta_L - y_L}{\sigma_N}\right). \tag{7}$$

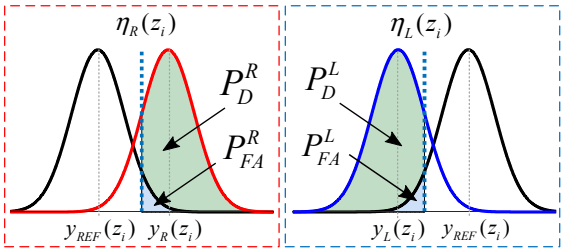

Fig. 2. Decision regions and probabilities for the two hypotheses tests. Recall that both the mean of the hypotheses and the decision thresholds depend on the observation sample z_i.

3.2 Detection performance

In order to analyze the detection performance, it is convenient to define two new parameters: the optical path loss (*OPL*) and dynamic range (*DR*) as

$$OPL^2(z_i) = f_e \frac{1}{N^2} 10^{-\frac{2\alpha z_i}{10}} \qquad DR = \frac{P_0 K W}{\sigma_N}. \tag{8}$$

The former combines all the power loss mechanisms at the distance z_i in the OTDR measurement, and the latter relates the OTDR parameters (peak power P_0, pulse width W and noise σ_N) and the backscattering coefficient K.

The mean value of the hypotheses y_{REF}, y_R and y_L can therefore be written in terms of the *OPL* and *DR* in Eq. (8), and the performance of the detection algorithm can be

analytically evaluated from the OTDR specifications. In the following, we fix a low false alarm probability $P_{FA}^{k} = 10^{-4}$ for both hypotheses tests, and we establish as a design criterion to have a probability of detection $P_{D}^{k} \geq 0.95$ for the given P_{FA}^{k}.

In Fig. 3(a) the achievable *OPL* is represented as a function of *DR* in the case of the Reflection Detection for different values of RL_e. It can be observed that even weak reflections do not require a high dynamic range to be detected. Figure 3(b) shows the maximum *OPL* for the Loss Detection in the backscattering (in solid line) and in the ONT_e reflection (in dashed lines) when assuming RL_{ONTe} = 40 dB. As it can be seen, the detection sensitivity is highly increased (about 11 dB). Consequently, the ONT reflection can be used in the coarse identification stage to rapidly check for fiber faults without requiring a high dynamic range.

It is clear that the ONT reflective termination significantly improves the detection sensitivity. To this respect, in Fig. 3(c), P_{D}^{L} is represented as a function of the ONT return loss. Here, the event insertion loss is 0.1 dB and it is assumed that the path loss to the ONT is 25 dB. As an example, to achieve the requirement of $P_{D}^{L} \geq 0.95$ with a *DR* = 25 dB, the ONT return loss should be lower than 41 dB. The sensitivity to the loss magnitude is shown in Fig. 3(d), where P_{D}^{L} is depicted as a function of IL_e when *DR* = 20 dB. For typical values of RL_{ONTe} = 40 dB, the sensitivity could be as high as 1 dB for an *OPL* = 25 dB.

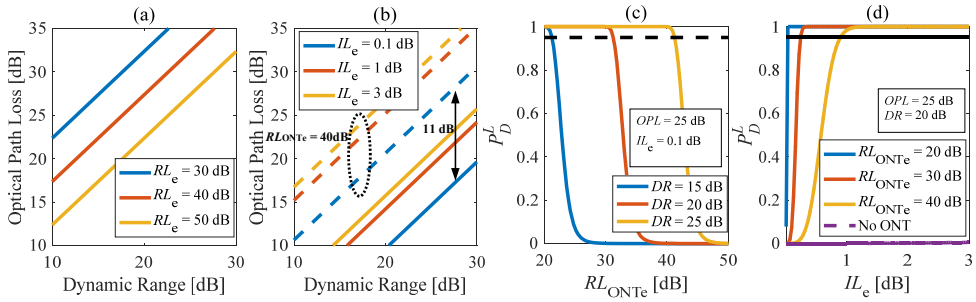

Fig. 3. Achievable *OPL* to detect (a) reflections and (b) losses (when $P_{FA} = 10^{-4}$, $P_D = 0.95$). Probability of loss detection versus (c) the ONT return loss and (d) the fault insertion loss.

4. DSPE-OTDR: event estimation

After the detection stage of the algorithm, the fault's characteristic parameters, RL_e and IL_e, which are deterministic values, are estimated from the samples where reflections and losses were detected, respectively.

Let us assume that either a reflection or a loss was detected at the samples $y(z_m)$, with *m* = 1, ..., *M*. If the noise is assumed independent and identically distributed, the *M* observation samples are statistically independent random variables. Thus, the likelihood function under the hypothesis *k* can be written as the product of the marginal probability density functions, given by Eq. (4), and the estimation problem may be written as

$$\hat{\theta}_k = \arg\max_{\theta_k} \ell(\theta_k), \tag{9}$$

where $\hat{\theta}_k$ is the estimator for RL_e and IL_e when $k = R, L$, respectively, and

$$\ell(\theta_k) = -\frac{1}{2\sigma_N^2}\sum_{m=1}^{M}\left(y(z_m) - y_k(z_m)\right)^2 \tag{10}$$

Optics EXPRESS

is the log-likelihood function under the hypothesis k, where y_k is function of the parameter θ_k. In Eq. (10), constants that are not involved on the estimation problem were omitted. By solving the optimization problem of Eq. (9), the maximum likelihood estimator (MLE) for the return loss $\widehat{RL}_e$ and the insertion loss $\widehat{IL}_e$ can be found to be, respectively (in dB)

$$\widehat{RL}_e = -10\log\left(\frac{\sum_{m=1}^{M}\left(y(z_m)-y_{REF}(z_m)\right)}{MP_0OPL^2(z_e)}\right), \tag{11}$$

$$\widehat{IL}_e = -5\log\left(\frac{\sum_{m=1}^{M}OPL^2(z_m)\left(y(z_m)-y_{REF}(z_m)\right)}{P_0WK\sum_{m=1}^{M}OPL^4(z_m)}+1\right). \tag{12}$$

In the case of the observation samples corresponding to the reflective termination, the MLE for the insertion loss is given by

$$\widehat{IL}_e = -5\log\left(\frac{\sum_{m=1}^{M}\left(y(z_m)-y_{REF}(z_m)\right)}{MP_0OPL^2(z_{\mathrm{ONTe}})10^{-\frac{RL_{\mathrm{ONTe}}}{10}}}+1\right). \tag{13}$$

It can be verified that the estimators in Eqs. (11)-(13) are consistent, i.e. they converge to their true values as the number of observation samples M increases, even if the fault is located in a dead zone or after a power splitter. For instance, while a fault with $IL_e =$ 1 dB after a 1:8 splitter will appear in the OTDR trace as a drop of 0.1 dB [15], from the proposed estimation procedure its real magnitude is directly obtained, in contrast to conventional OTDR analysis.

5. Proof-of-concept and experiments

The proposed DSPE-OTDR was experimentally probed using a commercially available OTDR with two laser sources at 1310 nm and 1550 nm and a test-bed PON deployed with standard single-mode fibers. The parameters of the OTDR and the fiber at 1550 nm are listed in Table 1. To estimate the noise standard deviation, we computed the histogram of acquired noise samples for different acquisition times. In Fig. 4(a) we show the noise histograms fitted with Gaussian functions for acquisition times of 1 and 3 minutes. Figure 4(b) shows the reflection from two ONT modules, from which we obtained their return loss. The first one, ONT_1, presents a lower return loss of RL_{ONT1} = 37.6 dB, while the second, ONT_2, has a higher return loss of RL_{ONT2} = 49.4 dB.

Table 1. Measured fiber and OTDR parameters

Fiber parameter	**Symbol**	**Value**
Backscattering coefficient (for T = 1 ns)	K	−82 [dB]
Attenuation coefficient	α	0.21 [dB/km]
OTDR parameter	**Symbol**	**Value**
Pulse peak power	P_0	31.8 [mW]
Source linewidth	$\Delta\lambda$	23 [nm]
Dynamic range (for T = 100 ns)	DR	Averaging 1 min: 19.16 [dB] Averaging 3 min.: 20.96 [dB]

Optics EXPRESS

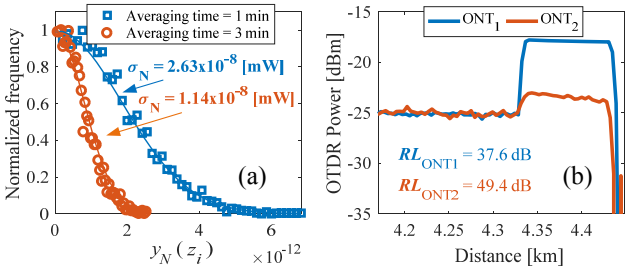

Fig. 4. (a) Histogram of OTDR noise for averaging times of 1 and 3 minutes, (c) measured reflection from the ONT.

The deployed test-bed PON is composed by a feeder fiber of 2.7 km, a 1:*N* power splitter and two branches are connected to it. The length of the drop fibers are $\{l_{\mathrm{DDFe}} = 6.2$ km, $l_2 = 2.93$ km$\}$, where the DDF$_e$ is composed by two fiber spools of 2.95 km and 3.2 km, joined by a LC connector, and it is terminated with the previously characterized ONT$_1$. The network topology was deliberately chosen in a way that the induced events, which are small in magnitude, lie within a dead zone, thus emulating pessimistic detection conditions. The reference traces for each test-bed PON were obtained by averaging over a large number of measurements previous to the operation. Note that while the reference signal will have a noise term, it will be very small since the noise variance decreases proportionally with the number of averages.

To choose the detection thresholds and the measurement parameters, such as pulse width and acquisition time, we set as a criterion that losses with a sensitivity of 1 dB must be detected with $P_D = 0.95$, given that $P_{FA} = 10^{-4}$. It is important to point out that the sensitivity can be arbitrarily increased, as we will see later, by properly choosing the OTDR acquisition parameters. Figure 5 shows the result of applying the DSPE-OTDR to different fault scenarios. Together with the current measurement, it is shown the reference trace (in dashed lines) and the samples where reflections (red dots) and losses (black dots) were detected.

In the first setup, the split-ratio of the PON is 1:32. Thus, the maximum *OPL* is composed by the splitting loss (~15 dB), the maximum propagation loss (~2.1 dB) and the overall insertion loss (~2 dB), which leads to *OPL* = 19.1 dB. From Fig. 3(b) it can be obtained that a dynamic range of *DR* = 24.9 dB is required. In our OTDR, this *DR* can be achieved, for example, using pulses of 500 ns and averaging over 3 minutes. Recall that shorter pulses, which lead to higher resolution, could be also used together with larger averaging times.

In the first place, we generated a misalignment in the LC connector of the DDF$_e$ inducing a real insertion loss of IL_e = 1.2 dB. Figure 5(a) shows the detection result of the DSPE-OTDR, where it can be seen that a strong reflection at the connector's location (at 5.7 km) is detected. The power loss induced by the event is also clearly detected in the waveform from the event to the ONT$_e$ localization. The estimation algorithm was subsequently applied and the event parameters were found to be $\widehat{RL}_e$ = 17 dB and $\widehat{IL}_e$ = 1.1 dB.

Optics EXPRESS

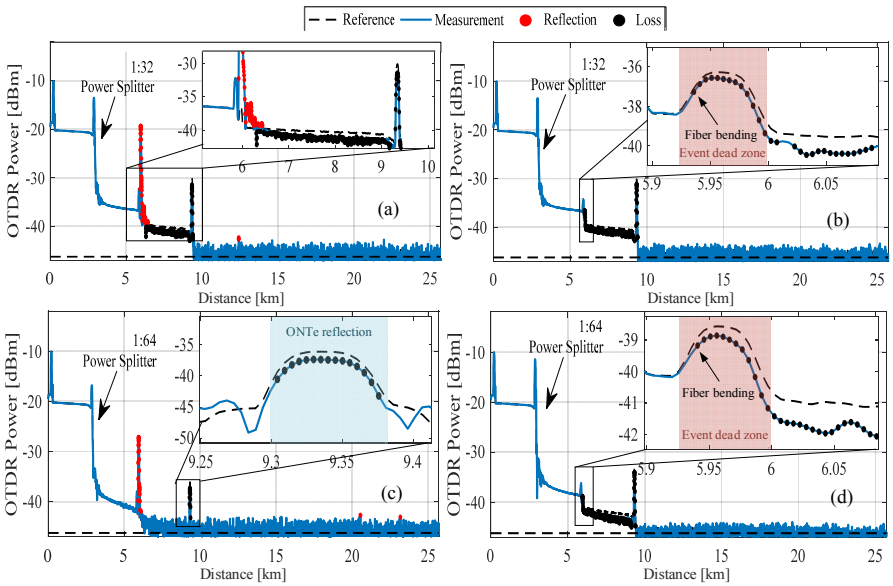

Fig. 5. Application of DSPE-OTDR in different scenarios: (a) a connector misalignment in a 1:32 splitter, (b) a fiber bending in a 1:32 splitter, (c) a connector misalignment in a 1:64 splitter and (d) a fiber bending in a 1:64 splitter.

Under the same scenario, a small fiber bending was generated a few centimeters after the connector of the DDF_e. Hence, the fiber bending lies in a dead zone and consequently it is not detected by the OTDR's own event-marking algorithm. However, as shown in Fig. 5(b), by applying the DSPE-OTDR it is accurately detected and the estimated value of IL_e is 0.94 dB.

The split ratio of the PON was next increased to 1:64 while the pulse width and acquisition times were kept fixed and the same faults were generated. In the case of the connector misalignment, the reflection is still clearly identified, but the dynamic range is not high enough to detect the losses in the backscattered signal. However, as depicted in Fig. 5(c), the loss is still detected at the ONT_e reflective termination and an accurate $\widehat{IL}_e = 1.18$ dB was obtained by means of Eq. (13).

In the same scenario, considering a low-loss non-reflective fault, such as a fiber bending, the loss is still detected at the reflective termination, and therefore the faulty branch can be identified. However, in order to localize such event within the PON, the OTDR measurement parameters should be adjusted in order to meet the requirements for the dynamic range. For instance, the maximum path loss in this scenario is $OPL = 22.2$ dB and hence, the required dynamic range to detect a loss of 1 dB in the backscattered signal, according to Fig. 3(b), is $DR = 27.9$ dB. In this example, to achieve this dynamic range we kept fixed the pulse width and increased 5 minutes the averaging time. The result is shown in Fig. 5(d), where the bending loss is accurately detected and it is estimated to have $\widehat{IL}_e = 0.97$ dB.

From the previous examples, it is clear how the proposed method can overcome the shortages of classical OTDR event-marking algorithms, providing a dead zone-free automatic event detection and accurate parameter estimation, even if small non-reflective faults after a power splitter are considered.

In the following, we show how using a dual-wavelength measurement, the type of fault can also be remotely identified from the estimated event parameters. To exemplify this, three common types of faults are considered: a link break, a connector misalignment providing finite insertion loss and a fiber bending. It is well known that in the case of a fiber/connector break, a high reflection and infinite insertion loss are induced. The wavelength dependence of

Optics EXPRESS

the mode-field diameter leads to a larger insertion loss at shorter wavelengths in a connector misalignment. On the other hand, the effective index in a fiber bending produces higher losses at longer wavelengths and negligible reflection [24,25].

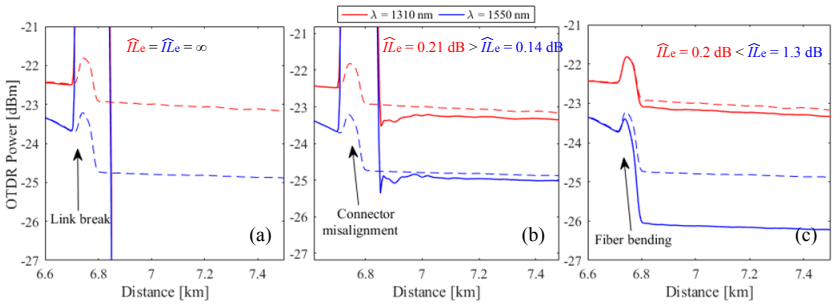

Fig. 6. OTDR signal and estimated insertion loss for (a) link break, (b) connector misalignment and (c) fiber bending.

Figure 6 shows the reference trace (in dashed line) and the measured trace after the event (in solid line) at wavelengths of 1310 nm and 1550 nm corresponding to a link break, a connector misalignment and a fiber bending. In this example, the *OPL* to the event is 15 dB, compatible with a 1:16 split-ratio. As it is expected, for a link break, a strong reflection is detected, and the estimated insertion loss at both wavelengths is very high and thus can be considered infinite. On the other hand, in a connector misalignment a relatively low insertion loss is induced. In this case, the estimated insertion loss at 1310 nm (0.21 dB) is found to be slightly larger than the one at 1550 nm (0.14 dB). Finally, in the case of the fiber bending, no reflection peak is detected and, as expected, the estimated loss is much larger at 1550 nm (1.3 dB) than the one at 1310 nm (0.2 dB). In this case, the absence of reflection and the loss magnitude at the two wavelengths allow to classify the event as a fiber bending.

5.1 DSPE-OTDR accuracy

In this section we assess the determination of the error in the measurement of the proposed scheme. When we estimate a parameter θ by some $\hat{\theta}$, there will be a nonzero estimation error, whose magnitude is a measure of the quality of the estimate, i.e. the accuracy of the DSPE-OTDR. While the same procedure can be followed to analyze the return loss estimation error, we will focus on the estimate for the insertion loss by means of Eq. (12) since, as we have seen, it plays an essential role in the task of the fault identification. Firstly, we define the variables

$$\widehat{IL}_e^* = 10^{-\frac{2\widehat{IL}_e}{10}} - 1 \qquad IL_e^* = 10^{-\frac{2IL_e}{10}} - 1, \tag{14}$$

where $\widehat{IL}_e$ is the estimate defined in Eq. (12), and therefore $\widehat{IL}_e^*$ is a random variable that follows a Gaussian distribution, since it is the sum of independent Gaussian random variables. On the other hand, IL_e and therefore IL_e^* are deterministic values, and hence we can define the error on the estimation as the difference, which is a random variable whose probability density function can be found to be

$$e = \widehat{IL}_e^* - IL_e^* \sim \mathcal{N}\left(0, \frac{\sigma_N^2}{\sum_{m=1}^{M}\left(OPL^2(z_m)P_0WK\right)^2}\right). \tag{15}$$

Optics EXPRESS

To guarantee that the absolute value of this error is not higher than ϵ with probability $1-\delta$, we require that $\Pr\{|e|<\epsilon\}=1-\delta$, which after some manipulations leads to an upper bound

$$\epsilon \le \frac{\sigma_N^2}{\sum_{m=1}^{M}\left(OPL^2(z_m)P_0WK\right)^2} Q^{-1}\left(\frac{\delta}{2}\right). \tag{16}$$

Notice that the estimation error decreases proportionally to the number of samples used for the estimation, which represents a great advantage respect to conventional OTDRs.

In order to compare the theoretical and experimental errors, we obtained a measurement with acquisition times of 30 seconds and 2 minutes after generating a loss inducing event with a real insertion loss of IL_e = 1.24 dB. In the acquired signals, which are partially shown in Fig. 7(a), the loss is detected at 680 observation samples. Thus, M of the samples ($M \le 680$) are used to obtain $\widehat{IL}_e$. In Fig. 7(b), it is depicted the experimentally obtained error by means of Eq. (15) (in circles) and the theoretical value of ϵ (in continuous line) as a function of M. Here, we fixed $\delta = 0.01$. Although in some cases the experimental error is slightly higher than the theoretical upper bound ϵ, it is always around this limit and following the theoretically expected trend. The slight deviations arise due to two main facts: the noise is not completely uncorrelated and the reference signal is not totally noise-free.

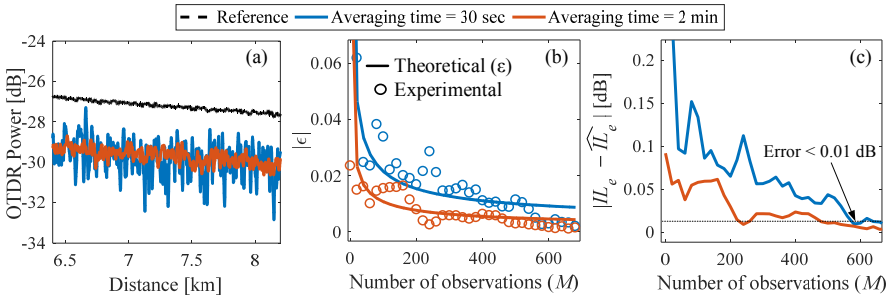

Fig. 7. Estimation error for the insertion loss: (a) samples used for the estimation, (b) theoretical and experimental error and (c) experimental estimation error in dB.

In Fig. 7(c), it is shown the experimentally obtained absolute error $\left|IL_e-\widehat{IL}_e\right|$ in dB units, which is the error of interest. When only one observation sample is used, the estimation error is 0.1 dB (for averaging time of 2 minutes) and 0.6 dB (for averaging time of 30 seconds). It can be seen how the estimation error rapidly decreases when more observation samples are used. For instance, using only M = 20 samples leads to an absolute error smaller than 0.05 dB, while for M = 600 samples, the error is less than 0.01 dB even for short averaging times of 30 seconds. This represents a measurement error much lower than that of conventional OTDRs, which are typically higher than 0.2 dB.

6. Multiple faults scenarios

The presented fault parameter estimation method was described for the case when a single impairment occurs in the network, which is the scenario with the highest probability of occurrence [15]. However, a PON monitoring system should be able to manage multiple-faults scenarios where several events arise between two consecutive measurements. In this section, we give a brief description of the supported fiber fault scenarios where for the sake of clarity we focus on the estimation of the faults' insertion loss.

Optics EXPRESS

Figure 8 shows different scenarios indicating possible fault locations and user distributions, highlighting the sample sections in the acquired signal where the loss arising from each fault have influence on the OTDR measurement. In the case of a single fault, as shown in Fig. 8(a), the estimators given by Eqs. (12)-(13) can be applied without any additional consideration.

Among the multiple-faults scenarios, one particular case occurs when there is no overlap between the losses generated by two events from different branches, as depicted in Fig. 8(b). In such a case, the insertion loss IL_1 and IL_2 corresponding to Fault-1 and Fault-2, respectively, can be individually estimated by applying the original Eqs. (12)-(13) over the appropriate influenced sample range, which are obtained from the coarse identification stage (recall that the coarse identification stage determines the number and distance to each fault).

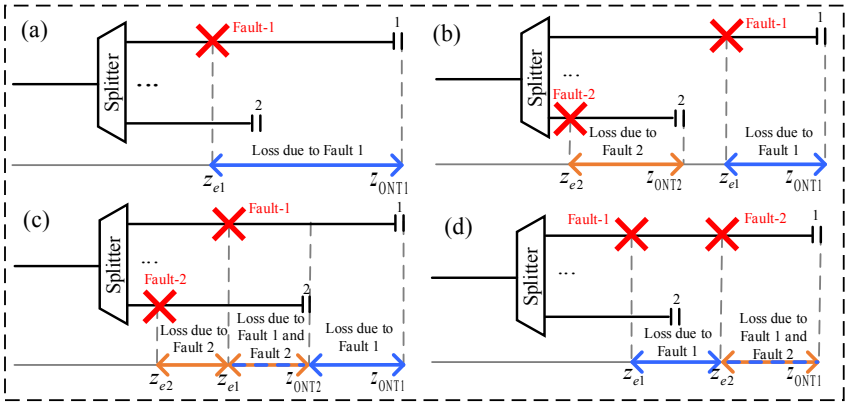

Fig. 8. Supported fault scenarios: (a) single fault, (b) multiple faults with no overlap, (c) multiple faults with overlap, (d) multiple faults in a single drop fiber.

When there is a partial overlap between the losses generated by multiple events from different drop fibers, the estimators must be slightly modified. In the example of Fig. 8(c) the insertion loss of Fault-1, IL_1, can be obtained by applying Eqs. (12)-(13) over the samples between z_{ONT2} and z_{ONT1}. In order to estimate IL_2 only the samples between z_{e1} and z_{ONT2} should be used by substituting the reference signal $y_{REF}(z_i)$ in Eqs. (12)-(13) by a new reference signal $y'_{REF}(z_i)$ that accounts for the estimated losses due to Fault-1 as

$$y'_{REF}(z_i) = y_{REF}(z_i) - f_1 \frac{1}{N^2} 10^{-\frac{2\alpha z_i}{10}} P_0 W K \left(10^{-\frac{2\widehat{IL}_1}{10}} - 1 \right). \tag{18}$$

That is, it is required to adjust the mean value of the null hypothesis by subtracting the estimated loss due to Fault-1. In this example, IL_2 can be estimated from the signal section between z_{e2} and z_{e1} if the coarse identification previously identified to which branch the fault belongs.

Finally, for the case of multiple faults in the same drop fiber, the application of the estimator of Eq. (12) over the different sample ranges gives the aggregated insertion loss. In the example of Fig. 8(d), by obtaining the insertion loss of Fault-1 and the total insertion loss, one can immediately determine the insertion loss due to Fault-2.

It is worth to mention that after a single failure, the most likely event is the breaking of multiple fibers at the same distance [15]. These type of events are easily recognized previously in the coarse identification stage and it is not necessary to use a more sophisticated

Optics EXPRESS

estimation criterion. For the rest of the multiple-faults scenarios, as those analyzed above, their relative probability of occurrence is relatively low.

7. Conclusions

In this work we presented the DSPE-OTDR, a novel OTDR-based fault analysis method suitable for remote monitoring of PONs. The proposed solution combines conventional OTDR techniques with a novel DSP scheme, which is a highly improved solution for characterization and identification of fiber faults, especially in optical access networks.

The detection stage identifies deviations with respect to the reference measurement. In our experiments, we are able to detect even small faults, such as a fiber bending or a connector misalignment, achieving high sensitivities: up to 0.14 dB in scenarios compatible with a split-ratio of 1:16 and higher than 1 dB in PONs with split-ratios up to 1:64. We also demonstrated the ability to detect such small faults when they are in an event dead zone, which are usually missed through conventional OTDR analysis.

The main advantage is that important fault parameters such as its insertion loss can be estimated with an accuracy higher than that obtained using conventional OTDRs, even if the fault is located after a power splitter. This allows the operator to completely characterize and identify the type of fault. As we demonstrated, the experimental error in the estimation of the insertion loss can be less than 0.01 dB even for short averaging times, in accordance with the theoretically expected behavior.

We also showed how the DSPE-OTDR can efficiently respond in multiple faults scenarios by slightly, but adequately, modifying the situation of a single fault.

To conclude, Table 2 summarizes the main features of the DSPE-OTDR and compare them with a conventional OTDR solution. As it is known, both methods allow the detection and characterization of the fault parameters in a point-to-point link (PtPL). For faults after a power splitter, the displayed loss in the OTDR trace is much smaller than the actual insertion loss and hence, the real magnitude of the event is missed. On the contrary, the DSPE-OTDR allows to find the real insertion loss of the event even for faults behind a power splitter. Additionally, the event parameters not only can be accurately estimated using the presented method, but also the type of fault can be identified, even if it lies in a dead zone.

Table 2. Comparison between conventional OTDR and DSPE-OTDR capabilities.

Capability	Conventional OTDR	DSPE-OTDR
Fault detection in PtPL	Yes	Yes
Fault parameter estimation in PtPL	Yes	Yes
Fault detection in PONs	Yes	Yes
Fault parameter estimation in PONs	No	Yes
Automatic fault identification	Some	Yes
Event dead zone-free operation	No	Yes
Event estimation accuracy	Medium/Low	High
Multiple fault operation	No	Yes

Since the presented approach operates over conventional OTDR profiles, it is completely scalable, transparent to data signals and it does not rely on the use of additional components in the ODN. In fact, only the OTDR processing software should be updated. This is extremely desirable from an operators' perspective since CAPEX and consequently OPEX are both greatly reduced compared to other monitoring solutions.

Funding

Universidad Nacional de Cuyo (C012, C014, C020), Consejo Nacional de Investigaciones Científicas y Técnicas (CONICET) (PIP 2017 No. 11220170101035CO), Comisión Nacional de Energía Atómica (CNEA) and Sofrecom Argentina SA.

Optics EXPRESS

References

1. G. Kramer, M. De Andrade, R. Roy, and P. Chowdhury, "Evolution of Optical Access Networks: Architectures and Capacity Upgrades," Proc. IEEE **100**(5), 1188–1196 (2012).
2. C. Mas Machuca, J. Chen, and L. Wosinska, "Cost-Efficient Protection in TDM PONs," IEEE Commun. Mag. **50**(8), 110–117 (2012).
3. M. A. Esmail and H. Fathallah, "Physical Layer Monitoring Techniques for TDM-Passive Optical Networks: A Survey," IEEE Comm. Surv. and Tutor. **15**(2), 943–958 (2013).
4. A. Ehrhardt, H. Foisel, F. Escher, A. Templin, and M. Adamy, "Monitoring of the transparent fibre infrastructure for FTTx networks: An operator's view," in *Proc. of IEEE Int. Conf. on Transparent Optical Networks (ITCON)* (2010).
5. B. Feigel, J. Van Erps, M. Khoder, S. Beri, K. Jeuris, D. Van Goidsenhoven, J. Watté, and H. Thienpont, "Optical Time-Domain Reflectometry Simulations of Passive Optical Networks: A Linear Time-Invariant System Approach for Arbitrary Pulses," J. Lightwave Technol. **32**(17), 3008–3019 (2014).
6. L. Wuilmart, V. Moeyaert, D. Daniaux, P. Megret, and M. Blondel, "A PC-based method for the localisation and quantization of faults in passive tree-structured optical networks using the OTDR technique," in *Proc. of IEEE Conf. on Lasers and Electro-Optics Society*, 122–123, (1996).
7. J. Laferriere, M. Saget, and A. Champavere, "Original method for analyzing multipath networks by OTDR measurement," in *Conference on Optical Fiber Communications*, 1997 OSA Technical Digest Series (Optical Society of America, 1997), paper TuT4.
8. H. Fathallah and L. Rusch, "Code-division multiplexing for in-service out-of-band monitoring of live FTTH-PONs," J. Opt. Net. **6**(7), 819–827 (2007).
9. M. P. Fernández, P. A. Costanzo Caso, and L. A. Bulus Rossini, "False Detections in an Optical Coding-Based PON Monitoring Scheme," IEEE Photonics Technol. Lett. **29**(10), 802–805 (2017).
10. M. P. Fernández, P. A. Costanzo Caso, and L. A. Bulus Rossini, "Design and performance evaluation of an optical coding scheme for PON monitoring," in *Proc. of XVI Workshop Info. Proc. & Control (RPIC)* (2015).
11. M. M. Rad, H. Fathallah, S. LaRochelle, and L. Rusch, "Computationally Efficient Monitoring of PON Fiber Link Quality Using Periodic Coding," J. Opt. Commun. Netw. **3**(1), 77–86 (2011).
12. X. Zhang, F. Lu, S. Chen, X. Zhao, M. Zhu, and X. Sun, "Remote coding scheme based on waveguide Bragg grating in PLC splitter chip for PON monitoring," Opt. Express **24**(5), 4351–4364 (2016).
13. K. Ozawa, M. Shigehara, J. Hanai, A. Ban, T. Naitou, and K. Shimoura, "Field trial of in-service individual line monitoring of PONs using a tunable OTDR," Proc. SPIE **4185**, 880–883 (2000).
14. K. Enbutsu, N. Araky, N. Honda, and Y. Azuma, "Individual fiber line testing technique for PON using wavelength assigned FBG termination and TLS-OTDR enhanced with reflected trace analysis method," in *Joint Conf. Opto-Electronics and Commun. Conf. and the Australian Conf. on Optical Fibre Tech.* (IEEE, 2008).
15. P. J. Urban, A. Getaneh, J. P. von der Weid, G. P. Temporão, G. Vall-llosera, and J. Chen, "Detection of fiber faults in passive optical networks," J. Opt. Commun. Netw. **5**(11), 1111–1121 (2013).
16. H. Iida, Y. Koshikiya, F. Ito, and K. Tanaka, "High-Sensitivity Coherent Optical Time Domain Reflectometry Employing Frequency-Division Multiplexing," J. Lightwave Technol. **30**(8), 1121–1126 (2012).
17. H. K. Shim, K. Y. Cho, Y. Takushima, and Y. C. Chung, "Correlation-based OTDR for in-service monitoring of 64-split TDM PON," Opt. Express **20**(5), 4921–4926 (2012).
18. Y. Luo, L. Xia, Z. Xu, C. Yu, Q. Sun, W. Li, D. Huang, and D. Liu, "Optical chaos and hybrid WDM/TDM based large capacity quasi-distributed sensing network with real-time fiber fault monitoring," Opt. Express **23**(3), 2416–2423 (2015).
19. G. C. Amaral, J. D. Garcia, L. E. Y. Herrera, G. P. Temporão, P. J. Urban, and J. P. von der Weid, "Automatic Fault Detection in WDM-PON With Tunable Photon Counting OTDR," J. Lightwave Technol. **33**(24), 5025–5031 (2015).
20. J. P. von der Weid, M. H. Souto, J. D. Garcia, and G. C. Amaral, "Adaptive Filter for Automatic Identification of Multiple Faults in a Noisy OTDR Profile," J. Lightwave Technol. **34**(14), 3418–3424 (2016).
21. M. P. Fernández, P. A. Costanzo Caso, and L. A. Bulus Rossini, "Effects of backscattering, dispersion, coherence and noise in a PON monitoring system," in *Proceedings of IEEE Biennial Cong. of Argentina* (IEEE, 2016).
22. X. Mei, F. Pang, H. Liu, G. Yu, Y. Shao, T. Qian, C. Mou, L. Lv, and T. Wang, "Fast coarse-fine locating method for φ-OTDR," Opt. Express **26**(3), 2659–2667 (2018).
23. S. M. Kay, *Fundamentals of Statistical Signal Processing* (Prentice Hall, 1993, Vol. 2: Detection Theory).
24. M. Cen, J. Chen, V. Moeyaert, P. Mégret, and M. Wuilpart, "Full monitoring for long-reach TWDM passive optical networks," Opt. Express **24**(14), 15782–15797 (2016).
25. W. Lee, S. I. Myong, J. C. Lee, and S. Lee, "Identification method of non-reflective faults based on index distribution of optical fibers," Opt. Express **22**(1), 325–337 (2014).